11th International Conference on Fracture Mechanics of Concrete and Concrete Structures
FraMCoS-11
J. M. Chandra Kishen, A. Ramaswamy, S. Ray and R. Vidyasagar (Eds)
https://doi.org/10.21012/FC11.092328

EXPERIMENTAL AND NUMERICAL STUDY OF FATIGUE DAMAGE IN HARDENED CEMENT PASTE AT THE MICROSCALE

YIDONG GAN[*], KLAAS VAN BREUGEL[*], ERIK SCHLANGEN[*], AND BRANKO ŠAVIJA[*†]

[*] Microlab, Delft University of Technology, Delft, the Netherlands
[†] e-mail: b.savija@tudelft.nl

Key words: Cement paste, Fatigue, Experiments, Lattice Modelling

Abstract: This contribution presents an experimental investigation and a numerical model of fatigue damage development in hardened cement paste at the micro-meter length scale. For the very first time, an experimental approach for measuring flexural fatigue of hardened cement paste specimens at the microscale has been developed. Microscopic cantilever specimens have been prepared and subjected to fatigue loading using a nanoindenter, with the aim of determining their fatigue life under different flexural stress levels (the so-called S-N curves). Compared to static fracture, microscopic images reveal an increased density of nano-scale cracks under fatigue loading. Based on the experimental data, a numerical model using a 2D lattice network approach for simulating the development of fatigue damage in hydrated cement paste at the microscale has been developed. The model uses segmented X-Ray computed tomography images as microstructural input. By assigning different mechanical and fatigue properties to different phases in the hydrated cement paste, it is possible to simulate the damage evolution in hardened cement pastes. A cyclic constitutive law is proposed for considering the fatigue damage evolution. The model is calibrated and validated using the experimental data from the tests described above and is shown to be able to reproduce well the flexural fatigue experiments in terms of S-N curves, stiffness degradation, and residual deformation. The proposed model can further be used as a basis for multi-scale analysis of fatigue in concrete.

1 INTRODUCTION

Over the past few years, many theoretical and numerical models have been proposed to study the fatigue of concrete. While most models focus on describing the macroscopic fatigue behavior of concrete, fatigue inherently involves multiple length scales. Therefore, there is an increasing interest in multiscale modelling of fatigue which could connect the heterogeneous material structures and properties at small scales with the macroscopic behavior of concrete. Most studies focused on the meso-scale, i.e., considering the material as a 3-phase composite comprising aggregates, ITZ, and cement paste. To date, however, there have been no attempts of testing and modelling fatigue of cement paste at the micro-scale. At this scale, the cement paste comprises mainly calcium hydroxide (CH), unhydrated cement (UHC), calcium silicate hydrate (C-S-H) and pores of various sizes. The present work aims at studying fatigue of hardened cement paste at this scale- the microscale- both experimentally and numerically.

To fill the knowledge gap, the fatigue bending tests on the micro-cantilever beams (MCB) of cement paste developed by the authors [1, 2] are carried out. X-ray computed tomography (XCT) technique is used to capture the initial material structure and assess the

fatigue damage accumulation of cement paste. A lattice-based fatigue model, which uses segmented XCT images as input, is proposed and used to simulate the development of fatigue damage in MCB fatigue tests.

2 EXPERIMENTS

2.1 Materials and methods

In this study, miniatured cement paste specimens are fabricated and scanned by XCT to obtain the realistic microstructure. Standard grade CEM I 42.5 N Portland cement is mixed with deionized water to prepare the cement paste. Two water-to-cement (w/c) ratios, 0.4 and 0.5, are used. After sealed curing for 28 days, the cement paste is cut by a precision micro-dicing machine (MicroAce Series 3 Dicing Saw) to generate micro-cantilever beams with a square cross section of 300 × 300 μm^2. The cantilevered length of the beam is around 1650 μm (Figure 1).

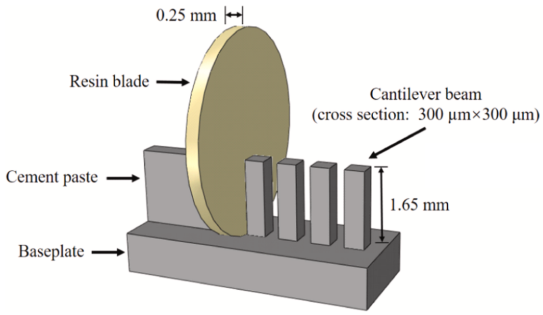

Figure 1. Schematic diagram of sample preparation.

Quasi-static and fatigue tests were performed using a KLA Nano- indenter G200. The Nano-indenter was equipped with a cylindrical wedge indenter tip with a length of 200 μm. It was used to apply vertical line loads at the free end of the MCB. The baseplate of MCB was attached on a metal surface using cyanoacrylate adhesive. The experimental set-up is schematically shown in Figure 2.

Before fatigue testing, the mechanical properties of MCBs, i.e., flexural strength and static elastic modulus, should be determined. For each w/c ratio, 30 cantilever beams were monotonically loaded to failure. The loading procedure was displacement-controlled with a constant loading rate of 50 nm/s. The load and displacement responses were measured by the Nano-indenter. In general, a major crack initiates near the fixed end of beam during the loading, which eventually leads to complete fracture of the beam. The maximum load F_{max} and slope of load–displacement curve k (in the range between 40% and 60% of the maximum load) during loading are respectively used to determine the flexural strength f_t and static elastic modulus E_{static} according to the classical beam theory.

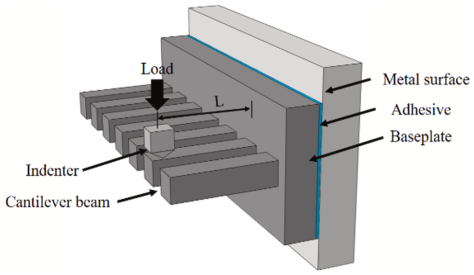

Figure 2. Schematics of the test setup.

The fatigue bending tests were carried out under load control. The cyclic loads were applied in the form of triangular loads with a constant amplitude at a loading frequency of 0.55 Hz. For each value of the w/c ratio, 30 MCBs were tested under different loading levels. For w/c 0.4 series, the maximum loading level ranges from 50 mN to 70 mN corresponding to around 75–95% of static flexural strength, and the minimum loading level is kept around 1.5–2.1 mN. The maximum loading level of w/c 0.5 series varies from 35 mN to 50 mN, which corresponds to approximately 70–95% of static flexural strength. The minimum loading level for this series is around 1.0–1.5 mN. The stress ratio R between minimum and maximum cyclic load was kept equal to 0.03. Due to the technical limitation of the testing duration of the used nano-indenter, the fatigue testing procedure was separated into multiple cycle blocks with identical loading procedure. Each cycle block contains 500 loading–unloading cycles and is automatically conducted in succession with a very short rest period (around 100 s). The beam is completely unloaded after finishing one cycle block and then reloaded for the next cycle

block. Run-out tests were stopped at the limit of 200,000 cycles.

2.2 Experimental results

Overall, the displacement evolution can also be divided into three stages: the first stage is unstable and comparatively transient, which occupies only 1–2% of the total loading procedure. With the proceeding of cyclic loading, displacement evolution curve turns into a stable stage, which covers around 99% of the whole test duration. In the third stage, the displacement grows rapidly within a few cycles until the MCB suddenly fails, which results in an overshoot of the indenter tip, as is shown in Figure 3.

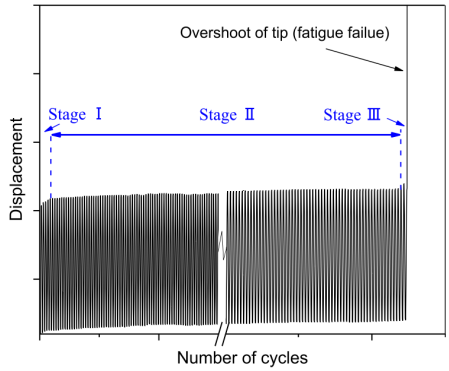

Figure 3. Typical displacement-cycles number curve.

The static mechanical properties as well as porosities of cement pastes measured by XCT for both w/c ratios at the age of 28 days are summarized in Figure 4. As was expected, a lower w/c ratio leads to higher elastic modulus and strength, mainly owing to the decreased porosity. Due to the highly heterogeneous nature of cement paste at the microscale, the results exhibit a wide variation. A general positive correlation between the E moduli and flexural strength is observed for both w/c ratios (Figure 4).

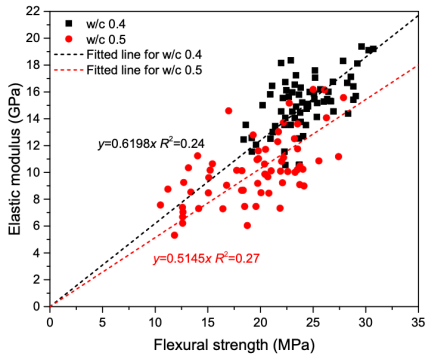

Figure 4. The relationship between the elastic modulus and flexural strength

The fatigue behavior of the MCB beams is characterized by S-N curves (Figure 5). This engineering approach is used for convenience, as negligible variation of sample strength is expected at the macroscale. However, despite the huge scatter inevitable in fatigue tests, the large variations of mechanical properties at the microscale may undermine the correctness and practicality of this method. To consider the individual variation of strength of each MCB, the initial elastic modulus (determined by the slope in the range of 40–60% of strength) measured before the fatigue test was used to predict the strength based on the linear correlation obtained in Figure 4. The results are given in Figure 6. The fatigue life for the same nominal stress level is rather scattered at the microscale, as is indicated by the low coefficients of determination (R^2). The results in Figure 6 show relatively high coefficients of determination after the variation of strength for individual sample is considered. For all modified stress levels, the fatigue life of w/c 0.4 sample is generally higher than that of w/c 0.5 sample.

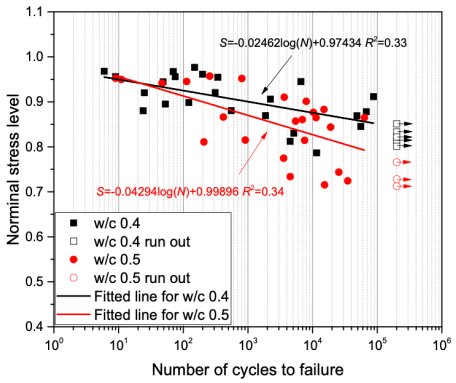

Figure 5. The nominal stress level versus number of cycles to failure.

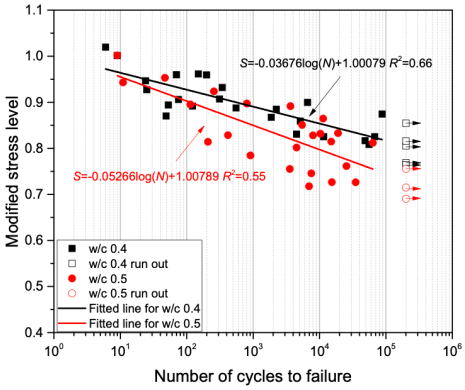

Figure 6. The modified stress level versus number of cycles to failure

The stiffness of MCB is determined by the slope of the ascending load–displacement curve under cyclic loading. For each w/c ratio, the variations of stiffnesses for 10 MCBs with the highest nominal stress levels were normalized to the initial stiffness (k_{int}) and plotted against the normalized number of cycles in Figure 7. Despite small fluctuations, the stiffnesses of most samples slightly decreased with cycles during the whole fatigue life, and some of them even remained almost unchanged before the fatigue failure. Unlike most macroscopic fatigue results of mortar or concrete samples [3-5], where distinct stiffness degradations of around 10–40% were observed and damage generated mainly at the interfacial transition zone (ITZ), the cement paste at the microscale seems to experience very slow and limited damage accumulation during most of the fatigue life. Once nano- or microcracks nucleate and form a major crack under cyclic loading, the MCB immediately fails. It turns out that a very small degree of fatigue damage is sufficient to cause a complete fatigue failure of MCB.

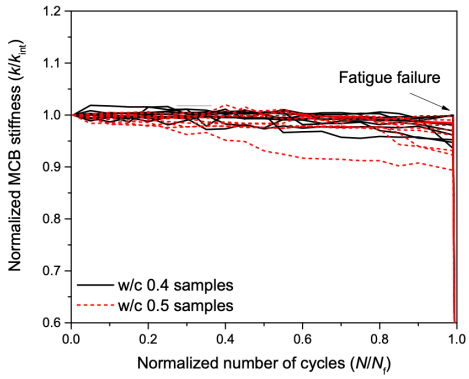

Figure 7. Stiffness degradations of 10 MCBs for each w/c ratio under cyclic loading.

3 MODELLING

3.1 Microstructure acquisition

Three beams for each w/c ratio were scanned using XCT to obtain greyscale-based 2D images (Figure 8). The X-ray source tube is set at 90 kV/100 μA during scanning, which results in a voxel resolution of 0.5× 0.5 × 0.5 μm^3. The segmentation procedure using the global thresholding method [6] is performed on these CT images. Four main phases, i.e., unhydrated cement (UHC), high-density (HD) C-S-H, low-density (LD) C-S-H and pores, can be distinguished after the segmentation. It should be mentioned that other hydration products, e.g., calcium hydroxide (CH), ettringite (AFt) and monosulfate (AFm), are not segmented in this study and consequently they are embedded in other segmented phases. Before the construction of the lattice network, the spatial resolution of XCT images is reduced to 5 μm/pixel using the bilinear interpolation algorithm to save computational time.

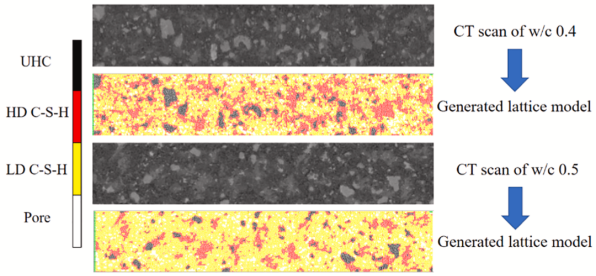

Figure 8. Segmentation of XCT images and generated lattice meshes for pastes with different w/c ratios.

3.2 Model formulation

As a first step, a lattice mesh needs to be generated. This is achieved by randomly positioning a lattice node within each pixel of the segmented XCT image. These nodes are then connected by a set of Timoshenko beam elements by performing a Delaunay triangulation. By assigning these beams with different properties, the microstructure of the material can be mapped on the lattice network. All beam elements are assumed to exhibit linear elastic brittle behaviour with different elastic modulus and maximum strength, depending on the XCT images.

When the model is subjected to the cyclic stress with the magnitude lower than the macroscopic strength, the lattice system will never fail. Therefore, a cyclic constitutive law incorporating the fatigue damage evolution is used here to consider the degradation of mechanical properties under fatigue loading. The fatigue damage of cementitious material mainly consists of the progressive growth of internal microcracks [7]. The growth of a microcrack manifests itself through degradation of macroscopic properties, such as stiffness. To account for this behaviour, the cyclic constitutive law for a lattice beam element is proposed, as is shown in Figure 9. The cyclic stress-strain curve for describing the mesoscopic fatigue behaviour is originally developed by Nagai et al. [8], and further modified by Gong et al. [9]. This cyclic law is similar to the continuous-function model developed by Hordijk [10] for simulating the post-peak cyclic behaviour of the crack in concrete.

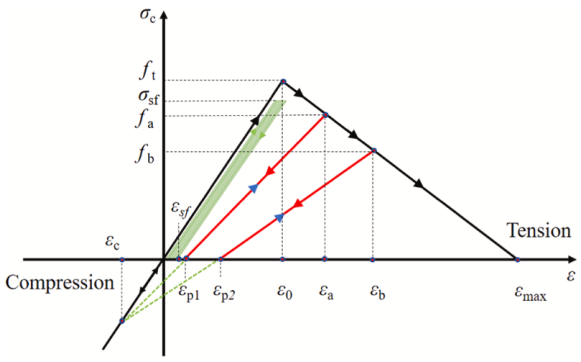

Figure 9. The constitutive law of individual lattice elements subjected to cyclic loading.

At each analysis step of the fatigue fracture simulation, the maximum fatigue load is imposed on the system. The comparative stress and corresponding stress level in every lattice element are calculated. Based on the stress levels and the number of cycles, the calculated fatigue damage in the form of mechanical degradation is then assigned into all damaged beams. For the unloading stage, it is assumed that the unloading process will not generate any damage such that the reloading curve (blue arrow) will overlap with the previous unloading curve (red arrow). Moreover, based on the experimental fact [2], there are always residual strains under cyclic loading. Therefore, the unloading curve in each loading cycle will not pass through the origin (Figure 9). After unloading, the system will be updated due to the new stiffness matrix and the remaining strength of each element. If the global stiffness of the system falls below 20% of its original stiffness, the simulation is stopped, and the system is considered to have failed. Otherwise, another analysis step is executed. Note that an analysis step does not always represent one loading cycle as is explained in next paragraph.

A beam is assumed to be purely linear elastic when in compression and neither compressive failure or compressive fatigue damage will not occur. Only the mechanical properties of beams that are subjected to comparative tensile stress will gradually decrease depending on the stress level and number of cycles. When in tensile, the pre-peak regime is characterized by the initial strength f_t and elastic modulus (f_t/ε_0) of the beam element. Each phase in cement paste is assigned with a fatigue property following the phenomenological S-N approach:

$$S_i = a \times \log N_i + b \quad (1)$$

Where S_i is the stress level of the element at the *i-th* analysis step; N_i is the corresponding fatigue life; a and b are two major parameters deciding the fatigue properties of hydrated cement paste phases. In this study, parameters a and b for different phases (low density and high density C-S-H) have been determined by fitting the simulation results to experiments. Based on this equation, the fatigue life can be calculated if the stress level is known.

Another important parameter is the fatigue

damage index D, defined as the reduction percentage of strength with respect to the initial strength of the element. Therefore, the remaining strength of the damaged element is calculated as $(1 - D)f_t$. When $D = 0$ the element is assumed to be undamaged, and when $D = 1$ the element will be removed from the mesh. Note that the same fatigue damage index is used for the elastic modulus of a damaged element in the current scenario. Generally, the fatigue damage D for each element should be accumulated with increasing number of cycles, and a higher stress level results in a higher degree of fatigue damage. Since the stiffness matrix is always updated due to the fatigue damage, the stress in the element will be redistributed in each loading cycle. Therefore, to consider the effect of redistribution of stress during the cyclic loading, the fatigue damage D_i at the *i-th* step is calculated based on the Miner's rule [11] and the fatigue damage at previous step D_{i-1}:

$$D_i = \frac{n_c}{N_i} + D_{i-1} \quad (2)$$

where n_c is defined as the cycle block for each analysis step and N_i is the fatigue life calculated from Eq. (1) based on the *i-th* step of stress level.

In general, a high-cycle fatigue test of cement paste under a moderate stress level involves tens of thousands of cycles. It is inefficient to explicitly simulate every loading cycle. Therefore, a proper accelerated strategy is preferred for fatigue damage simulation. To this end, the ''block cycle jump" technique, in which a certain number of cycles are packaged as one block loading case, is usually adopted [12]. Similarly, an appropriate number of cycles is chosen as the cycle block defined in Eq. (2) to speed up the fatigue simulation in this study. A value of 1000 is used for the cycle block herein.

The second case for considering the fatigue damage is that when the calculated highest stress level for the critical element exceeds 1 (i.e., $\sigma_{sf}/f_t > 1$): a post-peak cyclic softening behaviour is assumed for this element (Figure 9). In this case, the remaining strength of the element is gradually reduced following a linear softening curve [8,10]. For simplicity, only four softening steps are required for an element to reach the final fracture. At each softening step, a certain percentage of reduction d_{soft} in strength is assumed for this element, e.g. $f_a=(1 - d_{soft})\, ft$ and $f_b=(1 - d_{soft})^2 f_t$. Therefore, the fatigue damage index of this element at the *i-th* step should be $D_i = 1 - (1 - d_{soft})(1 - D_{i-1})$. Following the approach described in [9], a constant strain (ε_c =−400 με) at the compression branch is introduced for all phases to determine the reduction percentage of elastic moduli and the residual strains (e.g., ε_{p1} and ε_{p2}). When the maximum strain ε_{max} is also known, the residual strain ε_{p1} and the corresponding damaged elastic modulus E_{d1} of the element can be calculated using the following equations:

$$\varepsilon_{p1} = \frac{d_{soft}\varepsilon_c(\varepsilon_0 - \varepsilon_{max})}{\varepsilon_0 - \varepsilon_c} \quad (3)$$

$$E_{d1} = \frac{(1-D_i)f_t}{\varepsilon_a - \varepsilon_{p1}} \quad (4)$$

Note that UHC is assumed to have infinite fatigue life without fatigue damage accumulation.

Another important characteristic of fatigue test is the residual deformation. For each analysis step in the fatigue simulation, the local residual deformation of each element will be determined and then imposed on the lattice elements to calculate the macroscopic residual deformation. In this study, the change of strain at the maximum fatigue load is defined as the residual strain and the fatigue compliance is defined by dividing the residual strain by the half of the applied maximum stress.

For the case of $\sigma_{sf}/f_t > 1$, the residual deformation of the critical element is determined based on the post-peak cyclic behavior (Figure 9). If the stresses in all elements are lower than their strengths, the residual deformation of each element will be calculated considering the creep and fatigue crack growth. Bažant and Hubler [13] developed a theoretical model to relate the macroscopic deformation of concrete with the microscopic fatigue crack growth based on the Paris law. In this model, the total material compliance J_{tot} under cyclic loading is:

$$J_{tot} = J(t, t_0) + \Delta J_f \quad (5)$$

$$J(t, t_0) = \alpha_c \left(\frac{t - t_0}{t_1}\right)^{\beta_c} \quad (6)$$

$$\Delta J_f = C_t \times t \times f_{Hz} \left(\frac{\Delta\sigma}{f_t}\right)^{\gamma} \quad (7)$$

where $J(t,t_0)$ is the basic creep compliance given in [44,63]. It is defined as the creep strain at time t caused by a unit stress applied at the beginning time t_0. t_1 is the time unit. α_c and β_c are two creep parameters of each phase and ΔJ_f is fatigue compliance due to the crack growth. under cyclic loading [12]. The exponent γ is a constant with the value of 4 [13] and C_t is a fitting parameter [13]. $\Delta\sigma$ is the fatigue stress amplitude of the element and f_{HZ} is the loading frequency. Note that the current model is only applicable for the fatigue loading with a low loading frequency. When the higher loading frequency is used, the inertia effect of fatigue loading begins to play a role and should be considered.

More implementation details can be found in [14].

3.3 Modelling results

The experimental results in terms of S-N curves, stiffness degradations and residual deformation evolutions of MCBs have been used to calibrate the 2D flexural fatigue lattice model. As there is almost no other available experimental data for the cement paste at the microscale in literature, the validation is carried out by simulating samples that have not been used in the calibration phase. These samples differ in microstructures and w/c ratios. In the validation phase, parameter adjustment is not permitted. The calibration is first conducted on the sample with the w/c of 0.4 and the calibrated parameters for two C-S-H phases are summarized in Table 1.

The simulated S-N curves are compared with experimental results and shown in Figure 10. A wide variation of simulated fatigue life for different virtual samples can be observed in Figure 10. However, each virtual sample follows a unique linear S-N curve on the semi-log scale. It indicates that the major source of scatter in the result of fatigue simulation originates from the heterogeneous material microstructure. It is worth noting that another source of uncertainty for fatigue results comes from the determination of the true static strength, which is used to determine the nominal stress level. This problem can also be tackled in the simulations. Despite the large variation between individual samples, it has been clearly demonstrated that there is a significant difference in fatigue life for two w/c ratios, see Figure 10.

Table 1. Calibrated parameters for the fatigue model

Phases	HD C-S-H	LD C-S-H
a	0.02	0.04
b	1.1	1.1
α_C (10^{-6}/MPa)	0.23	0.34
β_C	0.20	0.20
C_t (10^{-6}/MPa)	5×10^{-6}	1.2×10^{-5}
ε_t ($\mu\varepsilon$)	3200	3200
d_{soft}(%)	20	20

Two examples of simulated fatigue fracture patterns are shown in Figure 11. Interestingly, multiple cracks have been observed for some fatigue flexural simulations, see the w/c 0.4 virtual sample in Figure 11. Similar findings have been found in experimental results reported in literature [15-18]: more diffuse microcracks have been detected in the specimens in fatigue tests compared to the static fracture tests.

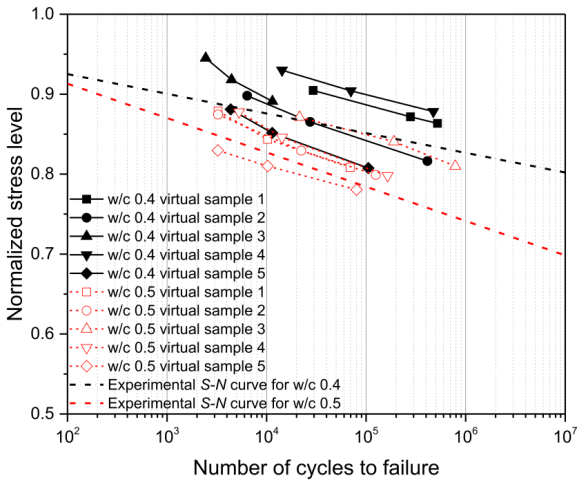

Figure 10. The simulated S-N curves for different virtual samples

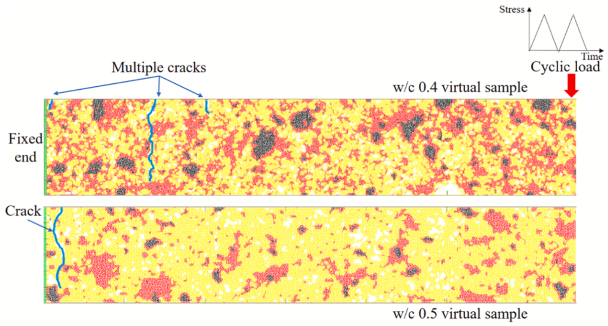

Figure 11. Examples of fatigue fracture patterns for w/c 0.4 and 0.5 virtual samples.

In general, the crack initiates at the weakest locations, e.g., LD C-S-H phases, under both static and fatigue loadings. The mechanical properties of each phase are important for the fatigue fracture behaviour. The major difference is that, when one propagating crack is impeded by other phases with higher fatigue resistances, i.e., HD C-S-H or UHC, this crack may branch or continue to propagate depending on the stress level, number of cycles as well as the accumulated fatigue damage in the surrounding phases. Since all C-S-H phases are simultaneously experiencing some degrees of fatigue damage in previous loading cycles and the fatigue damage evolution for HD C-S-H is much slower than that of LD C-S-H, some cracks may also initiate in LD C-S-H at other locations. Due to the updated global stiffness according to the fatigue damage accumulation, the stress redistribution will occur under each flexural cyclic loading and may lead to the presence of multiple cracks. However, it should be mentioned that this situation may only apply at the low stress level as the difference in fatigue life for two C-S-H phases is significant. When the stress in an element is slightly lower than its strength, the fatigue life for two phases is very close and only differs by some cycles. This may indicate different fatigue fracture behaviours at different stress levels. If the stress level is high enough, the fatigue fracture tends to be identical with the static fracture behaviour.

A typical stress-strain curve under the cyclic loading is presented in Figure 12. With the increasing number of cycles, the slope of the loading cycle gradually decreases.

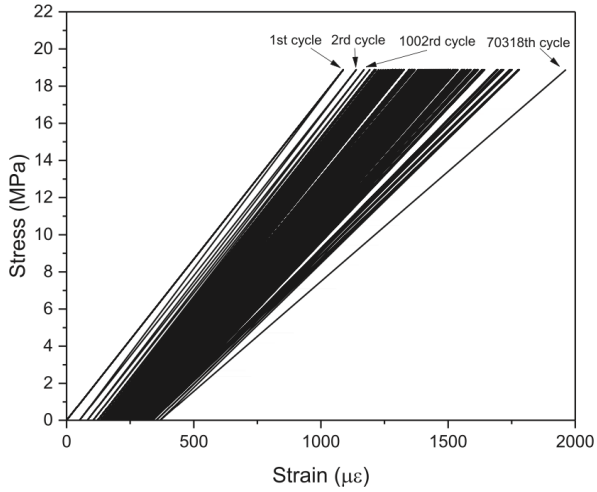

Figure 12. A typical simulated stress-strain curve for a w/c 0.4 sample under cyclic loading with the upper stress level of 90%.

The changes of the global elastic moduli for virtual samples, which represent the stiffness degradations under fatigue loading, are shown in Figure 13, along with the results of measurements. In most of the fatigue life the reduction of elastic modulus is very small. Overall, both the numerical and experimental results suggest a slow and limited flexural fatigue damage evolution process for cement paste at the microscale. Another important feature of fatigue fracture is that the fatigue crack becomes unstable when the total damage has accumulated to a certain degree. This is primarily because the remaining cross-section

of the specimen can no longer sustain the external fatigue loading. It is manifested as a sudden drop of stiffness, as is shown in Figure 13 (marked as blue lines).

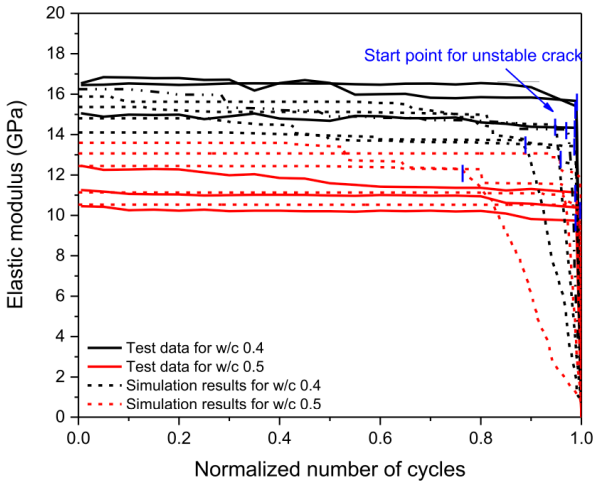

Figure 13. The simulated elastic modulus degradation compared with the experimental results.

4 CONCLUSIONS

Herein, fatigue experiments and simulations performed at the micro-meter length scale are presented. First, an experimental procedure for testing flexural fatigue on micro-cantilever beams has been developed and used. Then, a numerical model for simulating fatigue development of the micro-cantilever beams has been presented and validated. Based on the presented results, the following conclusions can be drawn:

- Given the same stress level, the fatigue life of cement paste at the microscale is almost two orders of magnitude longer than that at the macroscale, indicating a strong size dependency of fatigue in cement specimen.
- The microscopic fatigue damage evolution in cement paste is found to be very slow, indicated by the longer fatigue life as well as the less generated damage compared to the macroscopic fatigue of concrete.
- The proposed model can reproduce well the experimental results, in terms of S-N curve and stiffness degradation.

Since the development of fatigue damage in cement paste on the microscale is significantly slower than that of concrete on the macroscale, this indicates that the interfacial transition zone (ITZ) is potentially very important for initiation of fatigue cracks. This is further investigated in a follow-up study [19].

12 ACKNOWLEDGEMENTS

Yidong Gan would like to acknowledge the funding provided by China Scholarship Council (CSC), grant number 201706130140. Branko Šavija acknowledges the financial support of the European Research Council (ERC) within the framework of the ERC Starting Grant Project “Auxetic Cementitious Composites by 3D printing (ACC-3D)”, Grant Agreement Number 101041342.

REFERENCES

[1] Gan, Y., Vandamme, M., Chen, Y., Schlangen, E., van Breugel, K., & Šavija, B. , 2021. Experimental investigation of the short-term creep recovery of hardened cement paste at micrometre length scale. *Cement Concrete Res*. **149**: 106562.

[2] Gan, Y., Zhang, H., Zhang, Y., Xu, Y., Schlangen, E., van Breugel, K., & Šavija, B., 2021. Experimental study of flexural fatigue behaviour of cement paste at the microscale. *Int. J. Fatigue*. **151**: 106378.

[3] Chen, X., Bu, J., Fan, X., Lu, J., & Xu, L., 2017. Effect of loading frequency and stress level on low cycle fatigue behavior of plain concrete in direct tension. *Constr. Build. Mater*. **133**: 367-375.

[4] Fan, Z., & Sun, Y., 2019. Detecting and evaluation of fatigue damage in concrete with industrial computed tomography technology. *Constr. Build. Mater*. **223**: 794-805.

[5] Isojeh, B., El-Zeghayar, M., & Vecchio, F. J., 2017. Concrete damage under fatigue loading in uniaxial compression. *ACI Mater. J*. **114(2):** 225-235.

[6] Gan, Y., Romero Rodriguez, C., Zhang, H., Schlangen, E., van Breugel, K., & Šavija, B., 2021. Modeling of microstructural effects on the creep of hardened cement paste using an experimentally informed lattice model. *Comput. -Aided Civ. Infrastruct. Eng.* **36(5):** 560-576.

[7] Li, Q., Huang, B., Xu, S., Zhou, B., & Rena, C. Y., 2016. Compressive fatigue damage and failure mechanism of fiber reinforced cementitious material with high ductility. *Cement Concrete Res.* **90**: 174-183.

[8] Nagai, K., Sato, Y., & Ueda, T., 2004. Mesoscopic simulation of failure of mortar and concrete by 2D RBSM. *J. Adv. Concr. Technol.* **2(3):** 359-374.

[9] Gong, F., Ueda, T., Wang, Y., Zhang, D., & Wang, Z., 2017. Mesoscale simulation of fatigue behavior of concrete materials damaged by freeze-thaw cycles. *Constr. Build. Mater.* **144:** 702-716.

[10] Hordijk, D.A., 1991. *Local approach to fatigue of concrete.* PhD thesis, Delft University and Technology.

[11] E.W.C. Wilkins, *Cumulative damage in fatigue,* in: Colloq. Fatigue/Colloque Fatigue/Kolloquium Über Ermüdungsfestigkeit, Springer, 1956, pp. 321–332.

[12] Sun, B., & Xu, Z., 2021. An efficient numerical method for meso-scopic fatigue damage analysis of heterogeneous concrete. Constr. Build. Mater. **278:** 122395.

[13] Bažant, Z. P., & Hubler, M. H., 2014. Theory of cyclic creep of concrete based on Paris law for fatigue growth of subcritical microcracks. *J. Mech. Phys. Solids*. **63**: 187-200.

[14] Gan, Y., Zhang, H., Liang, M., Schlangen, E., van Breugel, K., & Šavija, B., 2021. A numerical study of fatigue of hardened cement paste at the microscale. *Int. J. Fatigue*. **151**: 106401.

[15] Le, J. L., Manning, J., & Labuz, J. F.. 2014. Scaling of fatigue crack growth in rock. *Int. J. Rock Mech. Min. Sci.* **72**: 71-79.

[16] Bažant, Z. P., & Xu, K., 1991. Size effect in fatigue fracture of concrete. *ACI Mater. J.* **88(4):** 390-399.

[17] Le, J. L., & Bažant, Z. P., 2011. Unified nano-mechanics based probabilistic theory of quasibrittle and brittle structures: II. Fatigue crack growth, lifetime and scaling. *J. Mech. Phys. Solids*. **59(7)**: 1322-1337.

[18] Toumi, A., Bascoul, A., & Turatsinze, A., 1998. Crack propagation in concrete subjected to flexural cyclic loading. *Mater. Struct.* **31**: 451-458.

[19] Gan, Y., Zhang, H., Liang, M., Zhang, Y., Schlangen, E., van Breugel, K., & Šavija, B., 2022. Flexural strength and fatigue properties of interfacial transition zone at the microscale. *Cement Concrete Comp*. **133:** 104717.